STRUCTURAL CHEMISTRY

ISSN 2053-2296

Salts of purine alkaloids caffeine and theobromine with 2,6-dihydroxybenzoic acid as coformer: structural, theoretical, thermal and spectroscopic studies

Mateusz Gołdyn,[a]* Anna Komasa,[a] Mateusz Pawlaczyk,[a] Aneta Lewandowska[b] and Elżbieta Bartoszak-Adamska[a]

[a]Faculty of Chemistry, Adam Mickiewicz University, Uniwersytetu Poznańskiego 8, Poznań 61-614, Poland, and [b]Department of Polymers, Faculty of Chemical Technology, Institute of Chemical Technology and Engineering, Poznan University of Technology, Berdychowo 4, Poznań 60-965, Poland. *Correspondence e-mail: mateusz.goldyn@amu.edu.pl

Received 2 August 2021
Accepted 19 October 2021

Edited by R. Diniz, Universidade Federal de Minas Gerais, Brazil

Keywords: pharmaceutical salts; neat grinding; microwave-assisted cocrystallization; supramolecular synthons; theobromine; caffeine; crystal structure; dihydroxybenzoic acid.

CCDC references: 1984555; 1984554

Supporting information: this article has supporting information at journals.iucr.org/c

The study of various forms of pharmaceutical substances with specific physicochemical properties suitable for putting them on the market is one of the elements of research in the pharmaceutical industry. A large proportion of active pharmaceutical ingredients (APIs) occur in the salt form. The use of an acidic coformer with a given structure and a suitable pK_a value towards purine alkaloids containing a basic imidazole N atom can lead to salt formation. In this work, 2,6-dihydroxybenzoic acid (26DHBA) was used for cocrystallization of theobromine (TBR) and caffeine (CAF). Two novel salts, namely, theobrominium 2,6-dihydroxybenzoate, $C_7H_9N_4O_2^+\cdot C_7H_5O_4^-$ (**I**), and caffeinium 2,6-dihydroxybenzoate, $C_8H_{11}N_4O_2^+\cdot C_7H_5O_4^-$ (**II**), were synthesized. Both salts were obtained independently by slow evaporation from solution, by neat grinding and also by microwave-assisted slurry cocrystallization. Powder X-ray diffraction measurements proved the formation of the new substances. Single-crystal X-ray diffraction studies confirmed proton transfer between the given alkaloid and 26DHBA, and the formation of N—H···O hydrogen bonds in both **I** and **II**. Unlike the caffeine cations in **II**, the theobromine cations in **I** are paired by noncovalent N—H···O=C interactions and a cyclic array is observed. As expected, the two hydroxy groups in the 26DHBA anion in both salts are involved in two intramolecular O—H···O hydrogen bonds. C—H···O and π–π interactions further stabilize the crystal structures of both compounds. Steady-state UV–Vis spectroscopy showed changes in the water solubility of xanthines after ionizable complex formation. The obtained salts **I** and **II** were also characterized by theoretical calculations, Fourier-transform IR spectroscopy (FT–IR), thermogravimetric analysis (TGA), differential scanning calorimetry (DSC) and elemental analysis.

1. Introduction

Research into different crystalline forms of active pharmaceutical ingredients (APIs) is one of the interests of chemists and engineers in the pharmaceutical industry. Each form of a given drug, such as polymorphs, solvates, hydrates, salts, cocrystals, amorphous forms, *etc.*, have different physicochemical properties due to the molecular arrangement in the solid state (*i.e.* stability, bioavailability, tabletability, permeability, mechanical properties and dissolution rate) (Carstens *et al.*, 2020). The preferred form of a substance is the crystalline form with the most stable arrangement of molecules (Ghadi *et al.*, 2014). In turn, amorphous substances have limited pharmaceutical use despite their proven better solubility compared to crystalline forms, due to their poor stability

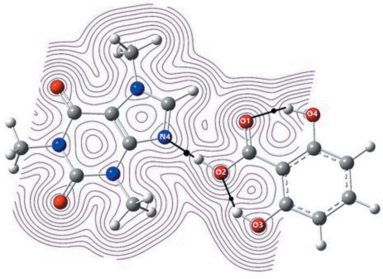

Table 1
Experimental details.

For both structures: $Z = 4$. Experiments were carried out with Cu $K\alpha$ radiation using a Rigaku OD SuperNova Single source diffractometer with an Atlas detector. Absorption was corrected by multi-scan methods (*CrysAlis PRO*; Rigaku OD, 2019). All H-atom parameters were refined.

	I	**II**
Crystal data		
Chemical formula	$C_7H_9N_4O_2^+ \cdot C_7H_5O_4^-$	$C_8H_{11}N_4O_2^+ \cdot C_7H_5O_4^-$
M_r	334.29	348.32
Crystal system, space group	Monoclinic, $P2_1/c$	Monoclinic, $P2_1/n$
Temperature (K)	132	131
a, b, c (Å)	6.9579 (3), 16.5845 (6), 12.4718 (5)	14.8560 (3), 6.95591 (11), 15.8927 (3)
β (°)	95.691 (4)	115.413 (3)
V (Å^3)	1432.06 (10)	1483.39 (6)
μ (mm^{-1})	1.06	1.05
Crystal size (mm)	0.34 × 0.24 × 0.08	0.3 × 0.17 × 0.12
Data collection		
T_{min}, T_{max}	0.649, 1.000	0.773, 1.000
No. of measured, independent and observed $[I > 2\sigma(I)]$ reflections	12055, 2970, 2782	11899, 3076, 2815
R_{int}	0.023	0.025
$(\sin \theta/\lambda)_{max}$ (Å^{-1})	0.631	0.630
Refinement		
$R[F^2 > 2\sigma(F^2)]$, $wR(F^2)$, S	0.055, 0.147, 1.11	0.034, 0.096, 1.05
No. of reflections	2970	3076
No. of parameters	273	290
No. of restraints	2	1
$\Delta\rho_{max}$, $\Delta\rho_{min}$ (e Å^{-3})	0.51, −0.24	0.28, −0.18

Computer programs: *CrysAlis PRO* (Rigaku OD, 2019), *SHELXT2018* (Sheldrick, 2015*a*), *SHELXL2018* (Sheldrick, 2015*b*) and *OLEX2* (Dolomanov *et al.*, 2009).

and the possibility of transformation into other phases (Hancock & Parks, 2000; Yu, 2001; Banerjee & Brettmann, 2020).

The search for the appropriate form of a drug is often difficult and time-consuming because, on the one hand, its pharmacological action must be maintained or improved and, on the other hand, its physicochemical properties, which have a direct impact on its activity, should be improved (Kumar & Nanda, 2018; Yadav *et al.*, 2009). Many methods are known to improve the physicochemical properties of an API, such as particle size reduction (Fang *et al.*, 2020), synthesis of solid dispersion (Nair *et al.*, 2020; Sareen *et al.*, 2012), nanoparticles (Kumar *et al.*, 2020), self-emulsifying drug delivery (SEEDS) (Pehlivanov, 2020), nanosuspension (Stefan *et al.*, 2020) or advanced lipid technologies (ALT) (Lopez-Toledano *et al.*, 2019). Another method is to introduce guest molecules into the crystal structure of an API, which is still a very popular method (Dai *et al.*, 2018). This gives an opportunity to create various types of two- or multi-component systems. One of these systems involves molecular complex formation, in which the molecules of both an API and a guest (coformer) are in the neutral form. When both of these substances and the complex which they form are in the solid form, under normal conditions, we can obtain a cocrystal (Byrn *et al.*, 2017). There is also the possibility of proton transfer between an API and coformer, leading to salt formation when certain conditions are met, such as a suitable ΔpK_a value or the structure of the compound (type and position of functional groups). The formation of complexes of this type (multi-component crystal) in comparison to pure substances (single-component crystal) most often leads to changes in physicochemical properties due to rearrangement of the molecules in the crystal lattice (Schultheiss & Newman, 2009).

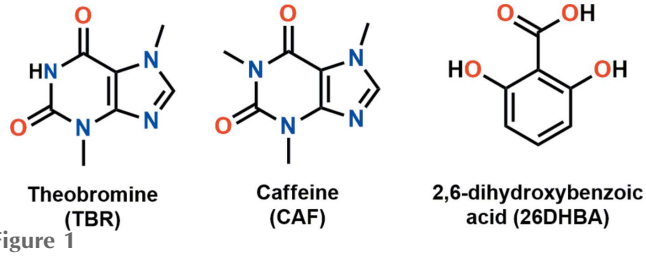

Figure 1
The structures of 2,6-dihydroxybenzoic acid and the alkaloids used for cocrystallization.

The use of acidic coformers with a given pK_a value for purine alkaloids containing an imidazole basic N atom may lead to the formation of an ionizable complex. In this article, 2,6-dihydroxybenzoic acid (26DHBA), the strongest of the dihydroxybenzoic acids, was used for cocrystallization with theobromine (TBR) and caffeine (CAF) (Fig. 1). The crystal structures of the title salts were determined by single-crystal X-ray diffraction. The powders were also characterized by powder X-ray diffraction, thermogravimetric analysis, differential scanning calorimetry, UV–Vis and Fourier-transform IR spectroscopy, and elemental analysis. Theoretical studies were also performed for the title salts.

2. Experimental

2.1. Materials

Theobromine (TBR) and caffeine (CAF) were purchased from Swiss Herbal and Coffeine Shop, respectively. 2,6-Di-

hydroxybenzoic acid (26DHBA) was obtained from TriMen Chemicals. All substances were used without prior purification. Millipore distilled water (18 MΩ) was used in all UV–Vis analyses.

2.2. Synthesis and crystallization

2.2.1. Cocrystallization from solution. Theobromine (13.3 mg, 0.074 mmol) and 2,6-dihydroxybenzoic acid (11.5 mg, 0.075 mmol) were dissolved in an isopropanol–water solution by heating, and single crystals of **I** were obtained by slow evaporation. Caffeine (27.5 mg, 0.14 mmol) and 2,6-dihydroxybenzoic acid (21.7 mg, 0.14 mmol) formed **II** by slow evaporation from an acetonitrile solution.

2.2.2. Cocrystallization by grinding. Neat grinding experiments were performed using an oscillatory ball mill Retsch MM300. TBR (8.8 mg, 48.8 µmol) with 26DHBA (7.5 mg, 48.7 µmol) and CAF (10.8 mg, 55.6 µmol) with 26DHBA (8.4 mg, 54.5 µmol) were ground with a 6.35 mm stainless steel ball. Each experiment lasted 30 min at a frequency of 25 Hz.

2.2.3. Microwave-assisted slurry cocrystallization. The Discover LabMate reactor was used as a microwave irradiation source for cocrystallization experiments. The alkaloid and the acid in stoichiometric ratios were placed in glass vials together with a magnetic stirrer bar, and then a specific volume of the appropriate solvent was added. Water, methanol, acetonitrile and ethyl acetate were used as solvents. The amounts of the substrates and solvents used in the microwave-assisted cocrystallizations are given in Tables S1 and S2 (see supporting information). The experiments with the slurries containing theobromine and 2,6-dihydroxybenzoic acid were carried out at 60 °C for 5 min with continuous stirring at 300 rpm. In turn, the experiments with samples containing caffeine were carried out at 80 °C for 3 min with a stirring speed at 300 rpm. The microwave potency needed to reach the desired temperature and maintain it during the reaction for a certain time was adjusted automatically by the apparatus. The solids obtained were dried under ambient conditions and characterized by powder X-ray diffraction (PXRD).

2.3. Refinement

Crystal data, data collection and structure refinement details for $(TBR\text{-}H)^{+}\cdot(26DHBA)^{-}$ (**I**) and $(CAF\text{-}H)^{+}\cdot(26DHBA)^{-}$ (**II**) are summarized in Table 1. H atoms were located in a difference Fourier map and refined with isotropic displacement parameters. In the final refinement model, chosen distances were restrained in both structures.

2.4. Powder X-ray diffraction (PXRD)

Low-temperature powder experiments using an Oxford Diffraction SuperNova diffractometer with a Cu $K\alpha$ radiation source for samples from a solvent, neat grinding and microwave-assisted slurry cocrystallizations were performed. *CrysAlis PRO* was used for data collection (Rigaku OD, 2019). Experimental conditions: scanning intervals = 0–50° (2Θ), time per step = 0.5 s and step size = 0.01° θ. Theoretical powder patterns were determined using *Mercury* (Macrae *et al.*, 2020). Parameters used for simulation: step size = 0.01° θ and width at half height (FWHM) = 0.2. The *Kdif* software (http://kdiff3.sourceforge.net/) was used for analysis of the powder patterns.

2.5. Vibrational spectroscopy (FT–IR)

FT–IR spectra were recorded in KBr pellets in the range 4000-400 cm^{-1} using a Bruker IFS 66v/S instrument, with a resolution of 2 cm^{-1}. Each spectrum was accumulated by the acquisition of 64 scans.

2.6. Theoretical calculations

Density functional theory (DFT) calculations were performed using the *GAUSSIAN16* program package (Frisch *et al.*, 2016). The APF-D hybrid DFT method including dispersion (Austin *et al.*, 2012) and the 6-311++G(d,p) basis set (Wiberg, 1986) were employed to obtain the optimized geometry and vibrational wavenumbers. The APF-D method was chosen as one of the best for determining the molecular geometry of organic molecules, hydrogen-bond interactions and IR spectra, and it had the best compromise between accuracy and computational cost (Foresman & Frisch, 2015). The X-ray geometries of **I** and **II** were used as starting points for the calculations. All calculated IR frequencies were real, which confirmed that the optimized structures corresponded to a local energy minimum. The potential energy distribution (PED) of the vibrational modes was established using the *VEDA 4* program (Jamróz, 2004, 2013). Only contributions to PED greater than 10% were considered.

2.7. Thermal analysis

The thermal stability of the described salts was investigated with a TG 209 F3 Tarsus thermogravimetric analyzer (NETZSCH–Geratebau GmbH, Norderstedt, Germany) in the temperature range from 30 to 600 °C. About 10 mg of sample was placed in a platinum crucible and analyzed with a 10 °C min^{-1} heating rate under a nitrogen atmosphere (purge of 10 ml min^{-1} of N_2 protection gas and 20 ml min^{-1} of N_2 sample gas). Melting temperatures (T_m) were measured by DSC (Mettler–Toledo DSC1 instrument, Greifensee, Switzerland) under a nitrogen atmosphere with a heating rate of 10 °C min^{-1} in the temperature range from 30 to 220 °C and were determined from the transition peaks.

2.8. Steady-state absorption spectroscopy

The concentrations of $(TBR\text{-}H)^{+}\cdot(26DHBA)^{-}$ (**I**) and $(CAF\text{-}H)^{+}\cdot(26DHBA)^{-}$ (**II**) in aqueous samples were determined *via* spectrophotometric assays using an Agilent 8453 UV–Vis spectrophotometer with a scanning range between 200 and 1000 nm, and 1 nm increments. The investigation of the solubility of the salts was performed using UV–Vis spectrophotometric assays. A series of standard solutions of **I** and **II** in distilled water at concentrations of 0.0025, 0.005, 0.01, 0.015 and 0.02 mg ml^{-1} were prepared and used for the preparation of the calibration curves. The recorded UV–Vis spectra exhibited maxima for **I** and **II** at 274 nm. The prepared

calibration curves were subsequently used for the calculation of the solubility of the salts by measuring saturated solution absorbance. Saturated samples of **I** and **II** were prepared by mixing 15 mg of the alkaloid derivative with 3 ml of distilled water at room temperature for 1 h, using an ultrasound bath. Saturation of the solutions was indicated by the presence of undissolved material. The spectrophotometric measurements were made in triplicate.

3. Results and discussion

3.1. Crystal structure design – Cambridge Structural Database (CSD) analysis

In the initial stage of designing the crystal structure of the two title substances, it was significant to know the forms in which they occur (neutral or ionized), the formation of possible supramolecular synthons and which of them are preferred. It was difficult to unequivocally predict the nature of the product based only on the determined ΔpK_a values for the discussed systems (Table 2), as they are in the range −1 to 4 (Cruz-Cabeza, 2012). However, much information can be gained by an analysis of solids containing substances that have been deposited in the CSD (Groom *et al.*, 2016) so far, which will be used for the cocrystal synthesis.

2,6-Dihydroxybenzoic acid is the strongest of the dihydroxybenzoic acids, due to the formation of two intermolecular hydrogen bonds in its structure, with the participation of the hydroxy groups and the carboxyl group (pK_a = 1.29) (Papadopoulos & Avranas, 1991). In the crystal structure of the pure acid, we observed either 2,6-dihydroxybenzoic acid molecules in which the carboxyl groups adopt the *syn* (motif C, monoclinic polymorph; Gdaniec *et al.*, 1994) or *anti* [motif D, orthorhombic polymorph (MacGillivray & Zaworotko, 1994) and monohydrate (Gdaniec *et al.*, 1994)] conformations (Fig. 2). In cocrystals of this acid, the carboxyl group more often adopts the *syn* (9 out of 10 entries) than the *anti* conformation (Table S4 in the supporting information) (Bruno *et al.*, 2002). This acid, however, is more likely to form salts than cocrystals. Of 50 deposited acid–base systems, 44 structures display proton transfer from 2,6-dihydroxybenzoic acid.

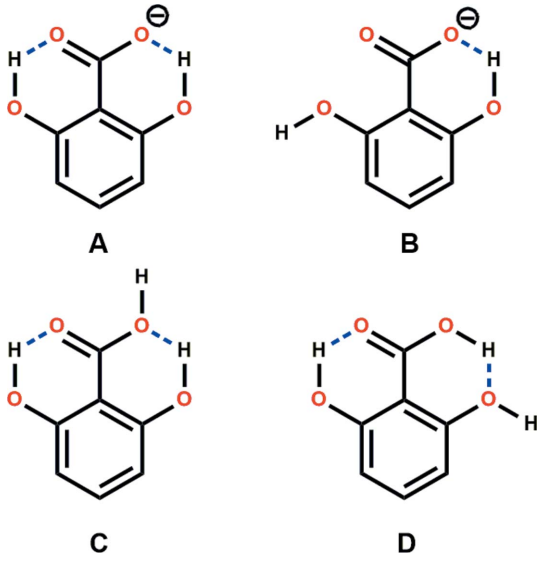

Figure 2
The observed motifs for the intramolecular hydrogen bonds in the 2,6-dihydroxybenzoate anion (motifs A and B) and 2,6-dihydroxybenzoic acid (motif C is the *syn*-COOH conformation and motif D is the *anti*-COOH conformation) (D'Ascenzo & Auffinger, 2015).

Table 2
Calculated ΔpK_a values for the title salts.

The 2,6-dihydroxybenzoic acid pK_a value of 1.29 was taken into account for the ΔpK_a calculation (Papadopoulos & Avranas, 1991).

Alkaloid	pK_a(protonated base)	ΔpK_a (Cruz-Cabeza, 2012) = pK_a(protonated base) − pK_a(acid)
TBR (theobromine)	0.12 (Pereira *et al.*, 2016)	−1.17
CAF (caffeine)	0.6 (Pereira *et al.*, 2016)	−0.69

In the two deposited structures where 2,6-dihydroxybenzoic acid is in the anionic form, only one intramolecular hydrogen bond with the participation of one hydroxy group was formed, while the proton from the second hydroxy group does not form any strong contact (motif B). However, the formation of two intramolecular noncovalent interactions with the participation of both hydroxy groups is much more preferable, as can be seen in 43 of 44 structures containing the 2,6-dihydroxybenzoate anion and in all structures where this acid is in the neutral form (Tables S3 and S4, respectively, in the supporting information). This observation is consistent with one of the Etter rules of the preferential formation of intramolecular hydrogen bonds over intermolecular interactions in six-membered rings (Etter, 1990). The hydroxy O atoms can also be proton acceptors if additional groups, such as nitrogen (*e.g.* $-NH_3^+$, primary or secondary amine group) or oxygen donors (*e.g.* –COOH or –OH group, or H_2O molecule), appear in their vicinity. In 22 entries containing the 2,6-dihydroxybenzoate anion, at least one hydroxy group acts as a proton acceptor and is involved in the formation of an intermolecular hydrogen bond (details are presented in Table S3 of the supporting information).

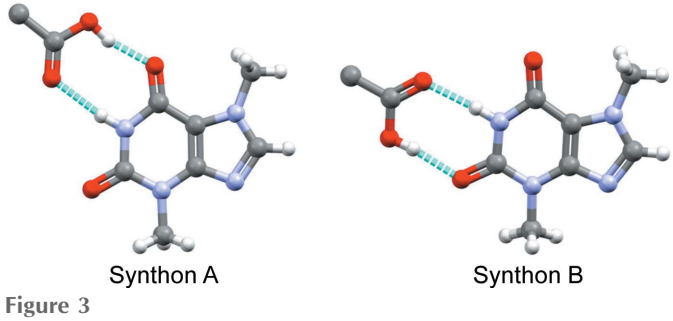

Figure 3
The supramolecular carboxylic acid–amide heterosynthons observed in theobromine–carboxylic acid systems. Synthons A [observed in structures with CSD refcodes UKOLAK (Gołdyn *et al.*, 2020) and CSATBR (Shefter *et al.*, 1971)] and B [HIJYEF (Karki *et al.*, 2007), MUPPET (Clarke *et al.*, 2010) and ZOYBOG (Jacobs & Amombo Noa, 2015)] represent synthons with the participation of the *exo*- and *endo*-carbonyl O atom, respectively.

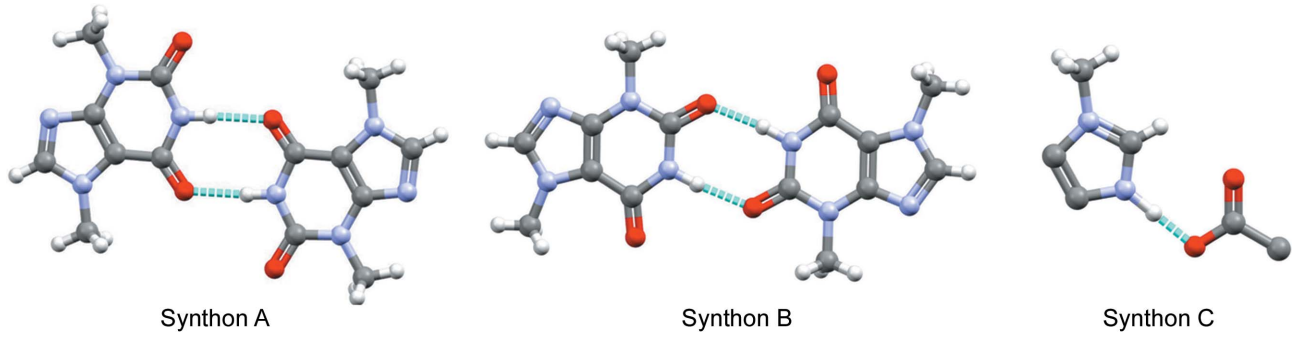

Figure 4
The predicted supramolecular synthons with theobromine (A, B and C) and caffeine (C). Synthons A and B represent amide–amide homosynthons with the participation of the *exo*- and *endo*-carbonyl O atom, respectively.

Caffeine has only good proton acceptors (carbonyl groups and an imidazole N atom) but does not have good donors. Theobromine, unlike caffeine, has one good donor at the pyrimidine ring. It can participate in the formation of strong amide–amide dimers, which are observed in many theobromine–carboxylic acid systems (Figs. 4*a* and 4*b*) (Groom *et al.*, 2016). The imidazole N atom of purine alkaloids most often interacts noncovalently with the carboxyl group of an acid. In several structures containing theobromine and a carboxylic acid derivative, formation of the amide–carboxylic acid synthon was observed (Figs. 3*a* and 3*b*). However, proton migration from the carboxyl group to the imidazole N atom is expected (Fig. 4*c*), so we do not take into account the possibility of the formation of an amide–carboxylic acid heterosynthon in the theobromine–2,6-dihydroxybenzoic acid system.

Based on the above considerations, it can be concluded with a high degree of probability that caffeine with 2,6-dihydroxybenzoic acid will form an ionized binary system maintained by N—H$\cdots$O$^-$ hydrogen bonding. In the crystal lattice of the theobromine–acid complex, it is envisaged that an imidazole–carboxylic acid motif (Fig. 4*c*) and the amide–amide homosynthon between two xanthine units will be observed. There are two possibilities for the formation of this dimer, *i.e.* with the *exo* or the *endo* carbonyl group of the pyrimidine ring of the alkaloid (Figs. 4*a* and 4*b*, respectively). The CSD analysis indicates the preference for the formation of the amide–amide synthon with the participation of the *exo*-carbonyl group (Groom *et al.*, 2016).

3.2. Synthetic approach

Cocrystallizations with theobromine and caffeine using 2,6-dihydroxybenzoic acid as coformer were performed. Theobromine with this acid can form a salt hydrate or a salt depending on the conditions of cocrystallization from solution or by milling. It has been shown that the monohydrate form (TBR-H)$^+$·(26DHBA)$^-$·H$_2$O was obtained by slow evaporation from an acetonitrile–water solution and by water-assisted grinding (Gołdyn *et al.*, 2019). In turn, cocrystallization by slow evaporation from an isopropanol–water solution leads to the anhydrous form (**I**). Caffeine with 2,6-dihydroxybenzoic acid forms only the salt (**II**). The described salt was obtained by cocrystallization in acetonitrile solution. A comparison of the powder patterns shows the possibility of the formation of both discussed compounds *via* grinding under solvent-free conditions (Figs. 5 and 6).

The use of microwave irradiation seems to be a promising method for obtaining cocrystals or salts. Both of the discussed compounds were obtained by microwave-assisted slurry cocrystallization. Solvents such as water, methanol, acetonitrile and ethyl acetate were used for these experiments. The powder diffraction patterns for the solids obtained by the synthesis using the above method were compared (Figs. 7

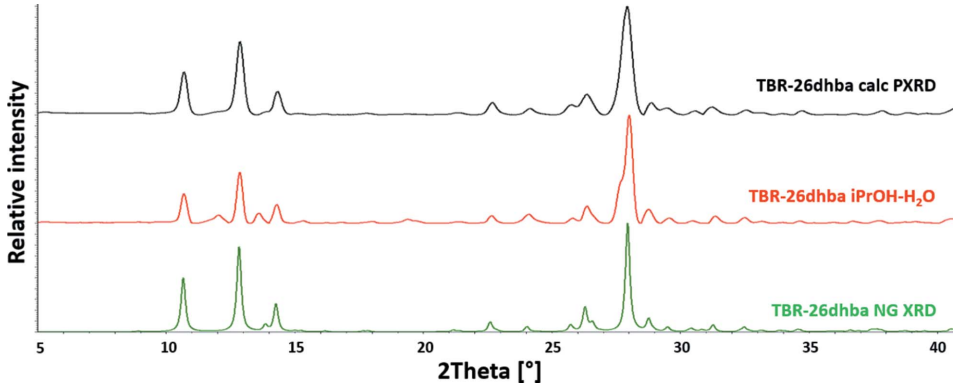

Figure 5
Comparison of the powder diffractograms for (TBR-H)$^+$·(26DHBA)$^-$. The theoretical powder pattern (black line) and the powder patterns of the materials from grinding (green line) and solution cocrystallization (red line) are presented.

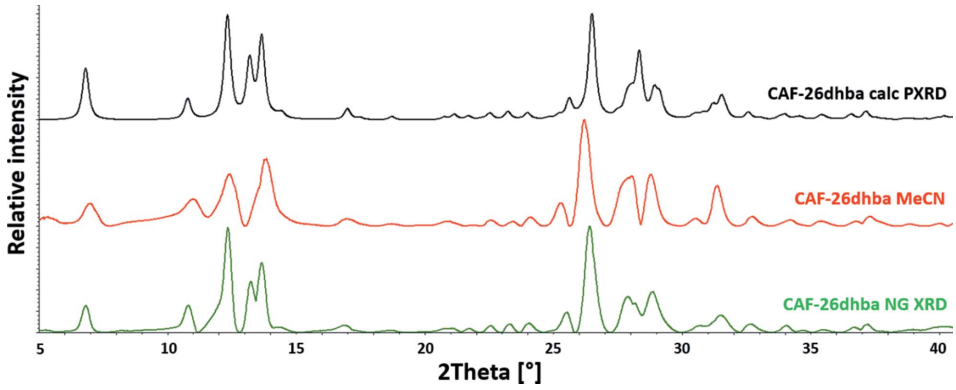

Figure 6
Comparison of the powder diffractograms for $(CAF\text{-}H)^{+}\cdot(26DHBA)^{-}$. The theoretical powder pattern (black line) and the powder patterns of the materials from grinding (green line) and solution cocrystallization (red line) are presented.

and 8). The microwave cocrystallization of caffeine and 2,6-dihydroxybenzoic acid in each case resulted in the formation of **II**. The use of water and acetonitrile to cocrystallize theobromine with this acid resulted in the desired product **I**. In turn, when methanol and ethyl acetate were used, peaks not only from salt **I**, but also from theobromine, were observed, which indicates incomplete conversion of the substrates. In these cases, the reaction should probably be carried out longer or at a higher temperature.

3.3. Structural analysis

Single-crystal X-ray diffraction measurements allowed the determination of the ionic nature of the title substances. The location of the proton in a difference Fourier map is the simplest determinant of the nature of the analyzed complex. However, we should also pay attention to the geometry of the relevant functional groups, since we are dealing with a pair of acid–base compounds. There is a significant difference in the C—O bond lengths in the carboxyl moiety, as opposed to the carboxylate anion, in which these values are similar.

In theobromine salt **I**, the C═O [C7—O1 = 1.241 (3) Å] and C—O [C7—O2 = 1.297 (3) Å] bond lengths suggest the presence of a carboxylate group. A similar situation occurs in caffeine salt **II**, where the difference in the C—O bond lengths in the carboxyl group of 2,6-dihydroxybenzoic acid is 0.041 Å [C7—O1 = 1.2530 (16) Å and C7—O2 = 1.2940 (15) Å]. Interestingly, such significant differences result from the different number of strong hydrogen bonds formed by the carboxylate O atoms and the nature of the donors (Chumakov *et al.*, 2006). In I and II, each of the carboxylate O atoms in the 2,6-dihydroxybenzoate anion forms strong intramolecular O—H···O hydrogen bonds, while one of them additionally forms a strong hydrogen bond with the imidazole N atom. The formation of the ionic complex is the result of proton migration from the acid group to the imidazole N atom, which is a basic group.

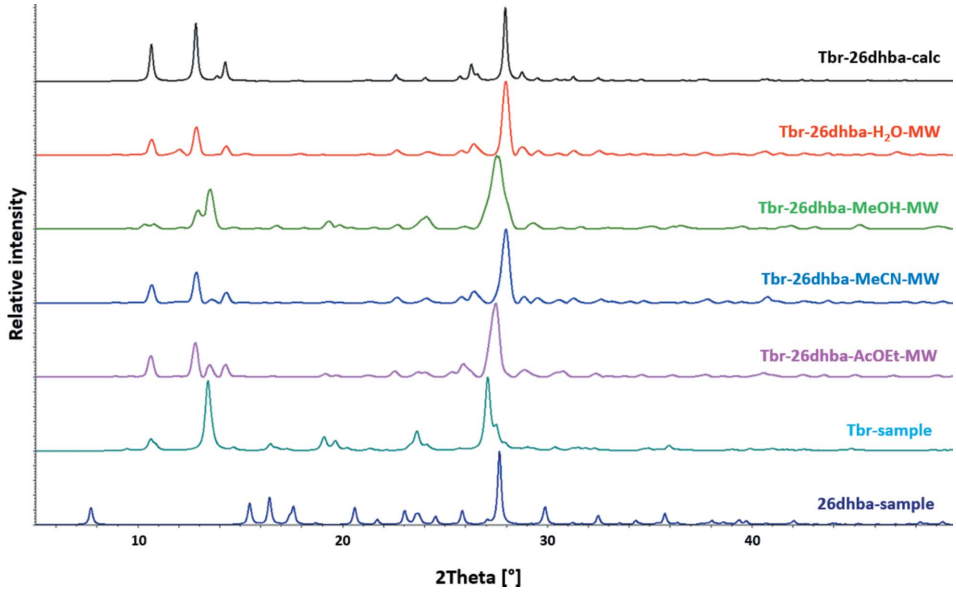

Figure 7
Compilation of the powder diffractograms for $(TBR\text{-}H)^{+}\cdot(26DHBA)^{-}$. The theoretical powder pattern and the powder patterns of the materials from microwave-assisted cocrystallization are presented. The powder diffraction patterns of the substrates are also included.

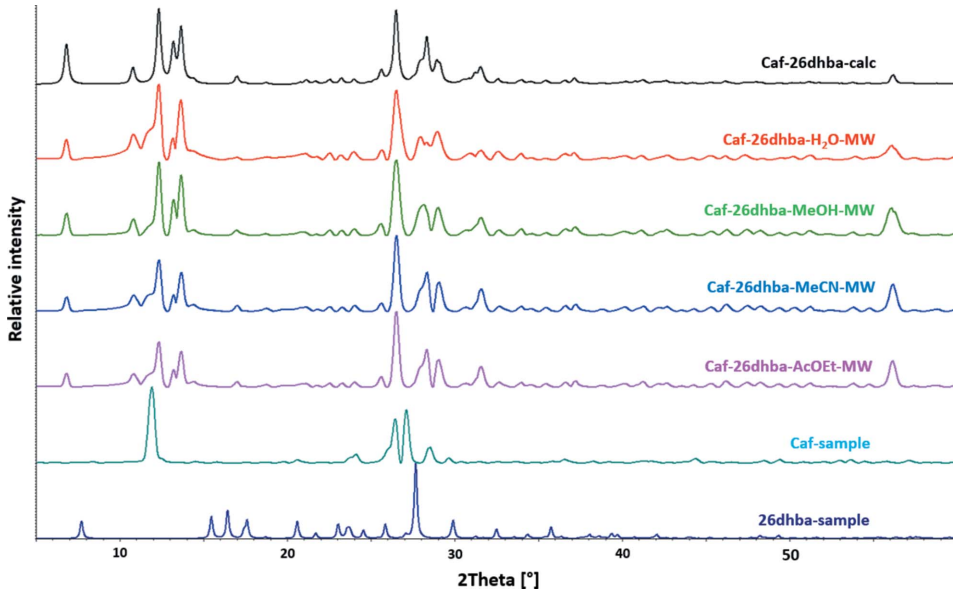

Figure 8
Compilation of the powder diffractograms for $(CAF\text{-}H)^{+}\cdot(26DHBA)^{-}$. The theoretical powder pattern and the powder patterns of the materials from microwave-assisted cocrystallization are presented. The powder diffraction patterns of the substrates are also included.

There is then a slight but distinct change in the geometry of the imidazole ring. Changes in the values of the valence angles in this ring can confirm the presence of the cationic form of the alkaloid molecule in the crystal lattice (Fig. 9). The list of values of the α, β and γ valence angles in the discussed complexes, together with those already obtained for theobromine and caffeine complexes with hydroxybenzoic acids, are presented in Tables S6 and S7, respectively, in the supporting information.

3.3.1. Theobromine with 2,6-dihydroxybenzoic acid. Theobromine and 2,6-dihydroxybenzoic acid cocrystallize as a salt, **I**, in a 1:1 stoichiometric ratio in the monoclinic space group $P2_1/c$ (Fig. 10*a*). In the crystal structure, finite four-component systems formed by two alkaloid and two acid molecules are observed (Fig. 10*b*). The hydroxy groups in the 2,6-dihydroxybenzoate anions are involved in intramolecular O—H···O^{-} hydrogen bonds and two $S(6)$ systems are formed (Table 3). As predicted, the acid–alkaloid motif is maintained through charge-assisted N—H···O^{-} hydrogen bonds (Fig. 4*c*). Each pair of theobromine cations forms a centrosymmetric $R_2^2(8)$ homodimer *via* N—H···O interactions with the participation of the *endo*-O atom (Fig. 4*b*). The above supramolecular motifs are consistent with earlier assumptions, however, a less expected amide–amide synthon is observed (Figs. 4*b* and 10*b*). Weak C—H···O hydrogen bonds and π(TBR)···π(26DHBA) interactions (Table S8 in the supporting information) are responsible for stabilization of the three-dimensional structure (Fig. 10*c*).

Table 3
Experimental and computed hydrogen-bond parameters (Å, °) in the TBR·26DHBA (**I** and **Ia**) and CAF·26DHBA (**II** and **IIa**) systems.

Alkaloid·26DHBA	*D*—H···*A*	*D*—H	H···*A*	*D*···*A*	*D*—H···*A*
Experimental **I**	O3—H3···O2	0.975 (10)	1.632 (16)	2.558 (2)	157 (3)
$(TBR\text{-}H)^{+}\cdot(26DHBA)^{-}$	O4—H4*A*···O1	1.00 (4)	1.62 (4)	2.550 (2)	153 (3)
	N1—H1···O6^{i}	0.85 (3)	2.04 (3)	2.881 (2)	169 (3)
	N4—H4···O2	0.94 (4)	1.62 (4)	2.557 (2)	169 (4)
Calculated **Ia**	O3—H3···O2	0.972	1.727	2.579	144
TBR·26DHBA	O4—H4*A*···O1	0.984	1.670	2.559	148
	O2—H4···N4	1.026	1.587	2.612	178
Experimental **II**	O3—H3···O2	0.94 (2)	1.72 (2)	2.5737 (13)	149 (2)
$(CAF\text{-}H)^{+}\cdot(26DHBA)^{-}$	O4—H4*A*···O1	0.91 (2)	1.69 (2)	2.5440 (13)	156.1 (19)
	N4—H4···O2	0.989 (15)	1.555 (15)	2.5441 (14)	179 (2)
Calculated **IIa**	O3—H3···O2	0.972	1.725	2.579	145
CAF·26DHBA	O4—H4*A*···O1	0.984	1.668	2.558	148
	O2—H4···N4	1.028	1.579	2.607	178

Symmetry code: (i) $-x+1, -y+1, -z$.

3.3.2. Caffeine with 2,6-dihydroxybenzoic acid. Caffeinium 2,6-dihydroxybenzoate salt **II** crystallizes in the monoclinic space group $P2_1/n$ with a caffeine cation and a $(26DHBA)^{-}$ anion in the asymmetric unit (Fig. 11*a*). These ionic species are hydrogen bonded *via* N—H···O^{-} interactions (Fig. 4*c* and Table 3). As expected, in the crystal structure of **II**, the alkaloid and acid form discrete two-component building blocks stacked in a 'head-to-tail' manner, sustained by π(CAF)···π(26DHBA) forces (Fig. 11*b* and Table S8). In the anion, two intramolecular O—H···O^{-} hydrogen bonds involving hydroxy groups are formed. The O3—C2—C3—C4 and O4—C6—C5—C4 torsion angles [−178.9 (1) and 179.8 (1)°, respectively] show that the phenol groups are practically in the same plane as the arene ring of the 2,6-dihydroxybenzoate anion. C—H···O interactions occur between neighbouring two-component building blocks and these additionally stabilize the $(CAF\text{-}H)^{+}\cdot(26DHBA)^{-}$ crystal structure (Fig. 11*c*).

3.4. Optimized structures and IR spectra

The optimized structures of the isolated molecules of TBR·26DHBA (**Ia**) and CAF·26DHBA (**IIa**) are

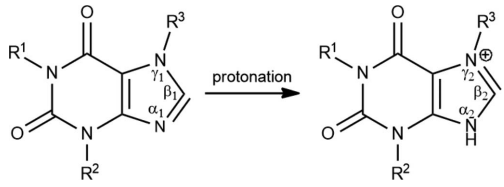

Figure 9
Changes in the values of the valence angles in the alkaloid imidazole ring as a result of proton transfer from the acid molecule to the imidazole N atom. It has been shown that the values of the α and γ valence angles are greater in the protonated forms ($\alpha_1 < \alpha_2$ and $\gamma_1 < \gamma_2$), while the value of the β valence angle decreases ($\beta_1 > \beta_2$) (Gołdyn *et al.*, 2021).

presented in Fig. S2 (see supporting information). The geometrical parameters (bond lengths, bond angles and selected torsion angles) are compared with the XRD results in Table S9.

The mean absolute differences (MAD) between the experimental and calculated bond lengths are 0.011 and 0.013 Å for **Ia** and **IIa**, respectively. The MAD of the bond angles for the theobromine complex is 0.94° and for the caffeine complex is 0.99°. In the crystal, the proton is transferred from the acid to the TBR or CAF molecule, which is in contrast to the isolated molecule. Additional calculations for CAF·26DHBA with acetonitrile or water (Fig. S2*c*) as solvents revealed also the transfer of the proton to the imidazole N atom. We conclude that the localization of the proton depends on intermolecular interactions.

Electron-density distribution can be described in detail with the quantum theory of atoms in molecules (QTAIM) (Bader, 1994; Lu & Chen, 2012). The (3,−1) critical points and the bonding paths between two atoms indicate the existence of hydrogen bonds. Bonding paths and critical points in the structures of **Ia** and **IIa** are shown in Fig. 12.

In order to interpret the measured IR spectra (Fig. 13), model spectra were calculated for the optimized structures. Details of these calculations are included in the supporting information (Figs. S3 and S4, and Tables S10–S13). For the

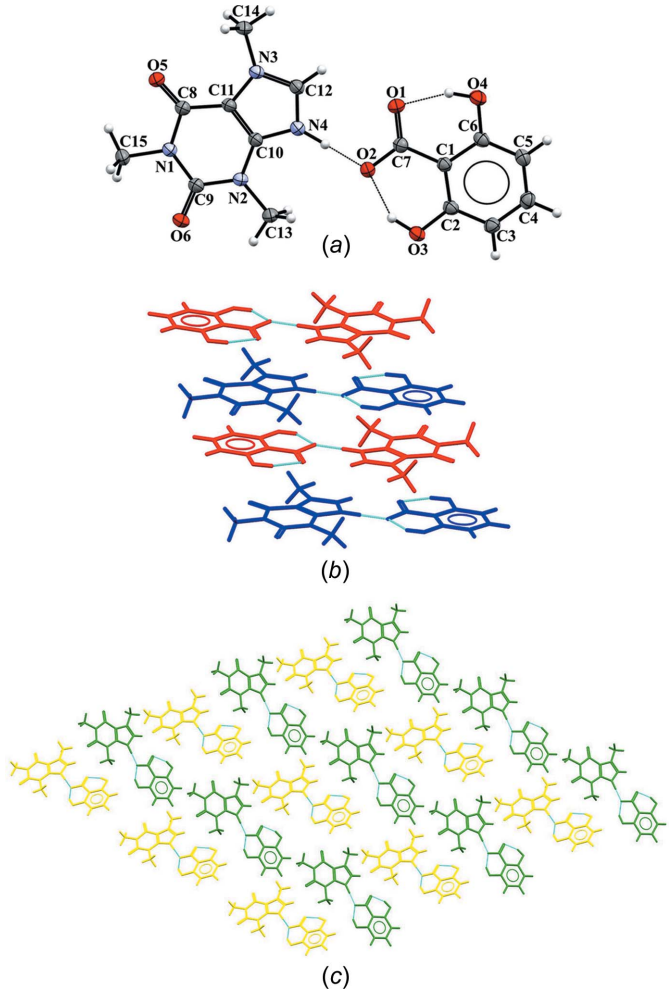

Figure 11
(*a*) The asymmetric unit of $(CAF\text{-}H)^{+}\cdot(26DHBA)^{-}$, with displacement ellipsoids drawn at the 50% probability level. (*b*) The two-component units interconnected by $\pi(CAF)\cdots\pi(26DHBA)$ forces. (*c*) The two-dimensional structure sustained *via* C—H···O interactions.

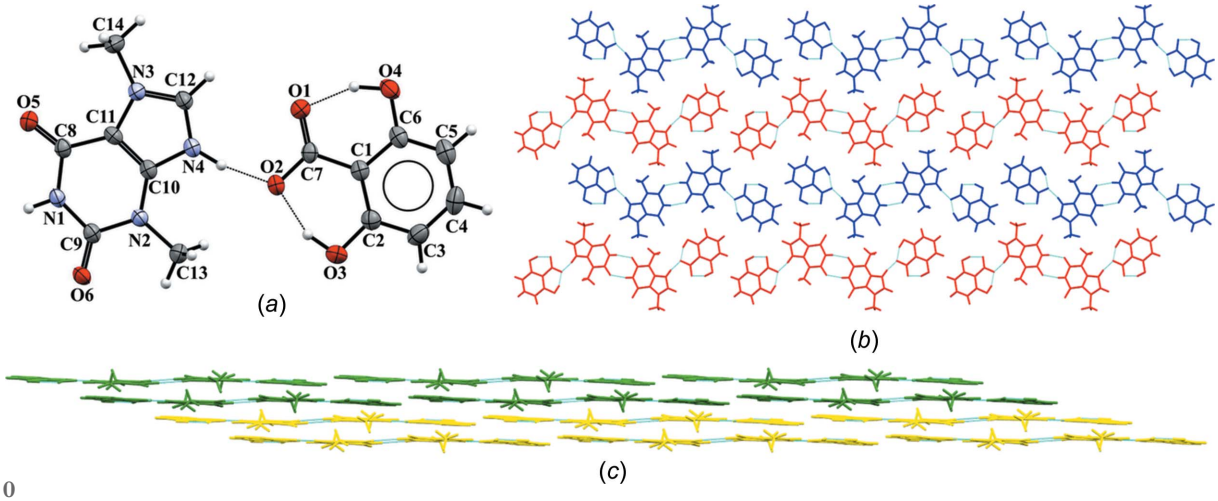

Figure 10
(*a*) The asymmetric unit of $(TBR\text{-}H)^{+}\cdot(26DHBA)^{-}$, with displacement ellipsoids drawn at the 50% probability level. (*b*) The 2D structure consisting of four-component systems of $(TBR\text{-}H)^{+}\cdot(26DHBA)^{-}$, interconnected by C—H···O hydrogen bonds. (*c*) The three-dimensional structure of **I** stabilized by $\pi(TBR)\cdots\pi(26DHBA)$ interactions.

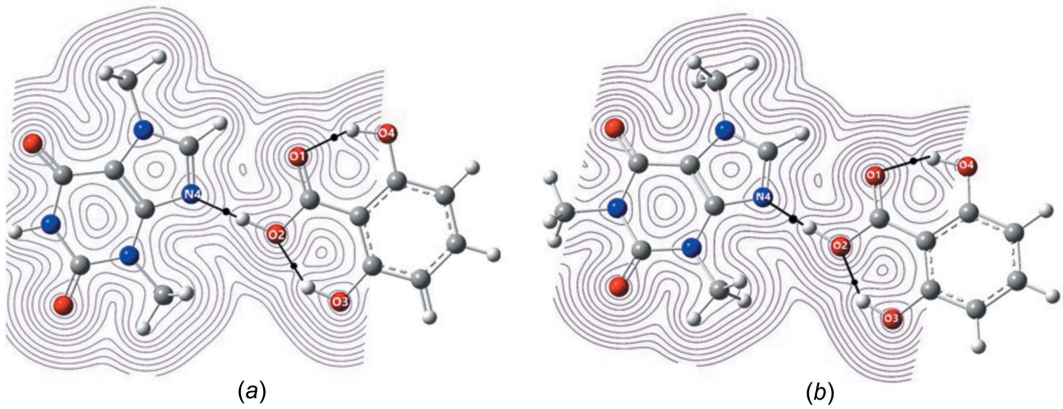

Figure 12
Critical points (black dots) and paths indicating interactions through hydrogen bonds for (*a*) TBR·26DHBA (**Ia**) and (*b*) CAF·26DHBA (**IIa**).

salts, in both cases, there are hydrogen bonds of medium strength, and in the experimental IR spectra, broad absorption with three ABC bands was observed. All bonds are noncentrosymmetric, especially N—H···O, hence the N—H stretching vibration bands are also visible. In salt **I**, in the range 3600–2000 cm^{-1}, the absorption is more intense compared to the spectrum of **II**, which is related to the presence of a weak N—H···O (2.881 Å) hydrogen bond in the TBR salt. The most intense band predicted theoretically is connected with the O—H···N mode.

The carbonyl group is characterized by a strong absorption band due to C═O stretching vibrations. In the IR spectrum of caffeine, two bands are observed in the carbonyl region at 1701 and 1660 cm^{-1} (Srivastava & Singh, 2013). After the formation of salt **II**, these bands are moved towards higher wavenumbers at 1718 and 1673 cm^{-1}, similar to the caffeine and theophylline complexes (Gunasekaran *et al.*, 2005). Stretching modes νCC and νCN in the purine ring are observed at 1565 and 1530 cm^{-1} for **II**, and at 1560, 1529 and 1516 cm^{-1} for **I**. The imidazole ring νCN vibrations are observed at 1322 cm^{-1}, whereas for TBR·26DHBA they are at 1335 cm^{-1}.

IR spectroscopy provides valuable information on salt formation. For 2,6-dihydroxybenozic acid, the νCOOH mode is observed at 1685 cm^{-1} (Solomon *et al.*, 2017). The formation of the salt causes the disappearance of this band and two bands are observed for the carboxylate anion. In the experimental spectra of **I** and **II**, carboxylate bands are observed at 1579/1390 and 1587/1390 cm^{-1}. Similar bands were observed for salts of 2,6-dihydroxybenzoic acid with nitrogen heterocycles (Solomon *et al.*, 2017) and Dapsone (Li *et al.*, 2020).

3.5. Solubility tests

The modification of active pharmaceutical compounds should lead to an improvement in their physicochemical properties. Much attention has been paid to solubility, an increase of which can affect other properties, such as permeability, bioavailability, dissolution rate and others (Roy & Ghosh, 2020). Solubility measurements were carried out for **I** and **II** using UV–Vis spectroscopy. Theobromine is characterized by relatively low solubility in water, *i.e.* 0.33 mg ml^{-1} (0.00183 mmol ml^{-1}). Cocrystallization of this alkaloid with 2,6-dihydroxybenzoic acid results in the formation of salt **I** with a solubility of 1.44 g l^{-1} (0.00431 mmol ml^{-1}) (Table 4). Thus, this compound is more than twice as soluble in water compared to the pure alkaloid. Earlier studies have shown that the monohydrate equivalent $(TBR\text{-}H)^{+}\cdot(26DHBA)^{-}\cdot H_2O$ has a 52-fold greater solubility than theobromine (Gołdyn *et al.*, 2019). The anhydrous form of this complex is less soluble than the hydrate analog, which shows that the presence of water in the crystal lattice can significantly improve water solubility.

Caffeine salt **II** shows a greater than 12 times lower water solubility (3.133 g l^{-1}, 0.009 mmol ml^{-1}) compared to pure caffeine (20.973 g l^{-1}, 0.108 mmol ml^{-1}). It is worth mentioning the salt hydrate of theophylline with this acid, which, according to UV–Vis studies by Sarma & Saikia (2014), is about 1.2 times more soluble in water than the pure alkaloid (Table 4).

Table 4
Comparison of the water solubility of the alkaloid derivatives with 2,6-dihydroxybenzoic acid described in the literature.

Alkaloid–26DHBA complex	Alkaloid solubility in water (mmol ml^{-1})	Absorption solubility (mmol ml^{-1})[a]
$(TBR\text{-}H)^{+}\cdot(26DHBA)^{-}$	0.00183 (Sanphui & Nangia, 2014)	0.00431 (×2.36) (this work)
$(TBR\text{-}H)^{+}\cdot(26DHBA)^{-}\cdot H_2O$		0.09452 (×51.65) (Gołdyn *et al.*, 2019)
$(TPH\text{-}H)^{+}\cdot(26DHBA)^{-}\cdot H_2O$	0.0457 (Sarma & Saikia, 2014)	0.0526 (×1.15) (Sarma & Saikia, 2014)
$(CAF\text{-}H)^{+}\cdot(26DHBA)^{-}$	0.108 (Lilley *et al.*, 1992)	0.009 (×0.083) (this work)

Note: (*a*) the change in water solubility in relation to the alkaloid solubility is shown in brackets.

3.6. TGA and DSC analysis

Thermogravimetric analysis (TGA) was used to investigate the thermal stabilities of $(TBR\text{-}H)^{+}\cdot(26DHBA)^{-}$ (**I**) and $(CAF\text{-}H)^{+}\cdot(26DHBA)^{-}$ (**II**). Theobromine salt **I** displays two decomposition steps. The first, occurring at 194 °C, can be attributed to the loss of 2,6-di-

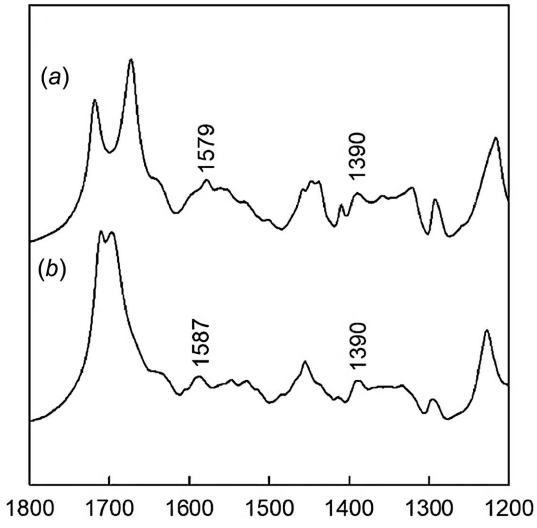

Figure 13
IR spectra in the range 1800–1200 cm^{-1} for (*a*) CAF·26DHBA and (*b*) TBR·26DHBA.

hydroxybenzoic acid (weight loss calculated 45.8%, determined 43.7%). The next step at 292 °C is the release of the alkaloid molecules (Fig. 14*a*). The melting point of this solid, determined by DSC analysis, is 202 °C (Fig. S5 in the supporting information). For comparison, the hydrate form (TBR-H)$^{+}$·(26DHBA)$^{-}$·H_2O melts at 193 °C (Gołdyn *et al.*, 2019). The decomposition of caffeine salt **II** is divided into two stages. The first step, related to decomposition of the acid, and the second, related to the decomposition of caffeine, are observed at 181.3 and 238.2 °C, respectively (Fig. 14*b*). However, it is not possible to determine the loss of mass occurring during the first stage, due to its continuity, and this, in turn, does not allow the method of decomposition of the caffeine salt to be determined. On the DSC curve, a sharp endothermic peak, indicating a melting point of **II**, is observed at T_m = 183 °C (Fig. S6). 2,6-Dihydroxybenzoic acid melts at about 173 °C (Liao *et al.*, 2010) and the melting points of the salts are between those of this acid and the given alkaloid [the melting points of caffeine and theobromine are 235.6 (Klímová & Leitner, 2012) and 348 °C (Martin *et al.*, 1981), respectively].

4. Conclusions

Cocrystallization of selected purine alkaloids with 2,6-dihydroxybenzoic acid as a coformer leads to the ionic complexes **I** and **II** in a 1:1 ratio. The reactions were carried out in solution, by milling and by microwave-assisted slurry cocrystallization, and the products obtained were confirmed by PXRD analysis. Structural studies showed practically complete success in obtaining the predicted basic supramolecular synthons responsible for the noncovalent association of molecules in the described purine derivatives. Both hydroxy groups in the 2,6-dihydroxybenzoate anion form intramolecular O—H···O^{-} hydrogen bonds. Proton migration from the carboxyl group to the imidazole N atom, confirmed by the presence of the carboxylate group and the imidazole-ring geometry, leads to N—H···O^{-} hydrogen-bond formation (alkaloid–acid heterosynthon). However, the amide–amide dimer found in **I** was not formed with the *exo*-carbonyl group but with the *endo*-carbonyl group, which is less frequently observed in theobromine–carboxylic acid systems.

Following the assumptions based on the ΔpK_a values and an analysis of the CSD, ionic complexes were obtained. Theoretical calculations carried out for the isolated system reflected the structure obtained by the single-crystal X-ray diffraction method, apart from the proton transfer from the 2,6-dihydroxybenzoic acid to the alkaloid molecule. The difference in the nature of the compounds obtained by the above methods may result from the role of intermolecular interactions in the solid, which are not taken into account in theoretical calculations. Only additional calculations in which proton transfer was simulated in the presence of a solvent as

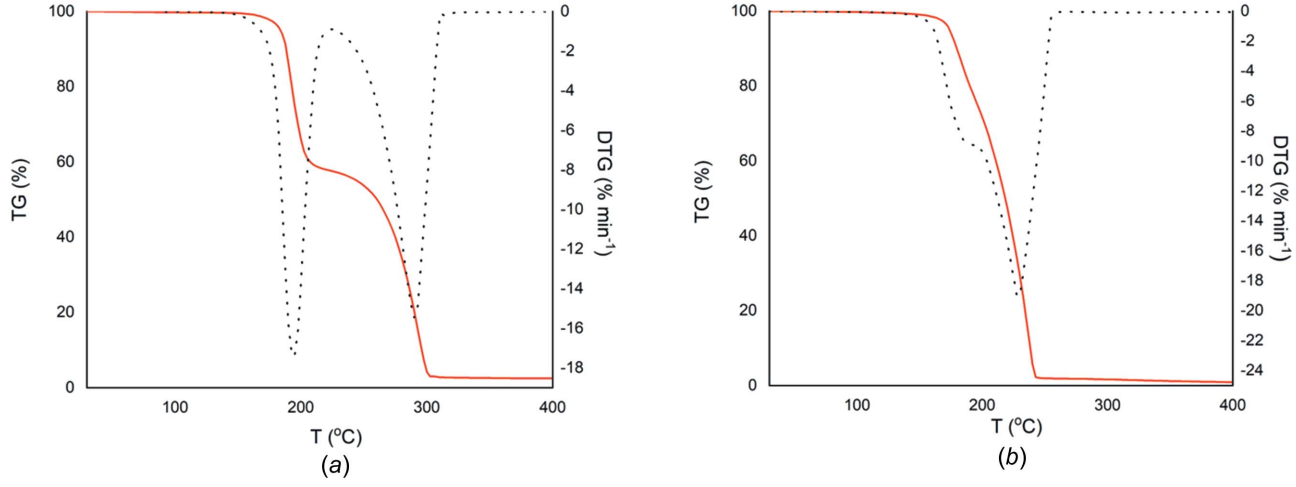

Figure 14
TG (solid red line) and DTG (dotted black line) curves for (*a*) (TBR-H)$^{+}$·(26DHBA)$^{-}$ and (*b*) (CAF-H)$^{+}$·(26DHBA)$^{-}$ over the temperature range 30–400 °C.

an environment (acetonitrile or water) gave results consistent with our results and the literature data. IR spectroscopy further confirmed the formation of the salts.

Theobromine with 2,6-dihydroxybenzoic acid forms a salt monohydrate (1:1:1 ratio) or anhydrous salt **I** (1:1 ratio) depending on the cocrystallization conditions. Both are more soluble in water than the pure alkaloid by 2.4 and 52 times, respectively. Caffeine forms anhydrous ionic complex **II** with this acid, which is 9 times less soluble in water than caffeine. Theophylline forms with 2,6-dihydroxybenzoic acid a slightly more water-soluble salt hydrate (1:1:1 ratio).

In addition to the above differences, we also observed different thermal properties. Both salts described in this article have melting points higher than the melting point of the coformer but lower than the melting point of the alkaloid. The decomposition of both complexes takes place in two stages, with the release of acid molecules in the first stage. In contrast to the theobromine salt, the release of acid coincides with the degradation of the alkaloid in the caffeine salt, so it was impossible to determine a definite way of this salt decomposition.

Acknowledgements

MG and MP acknowledge financial support from the European Union through the European Social Fund under the Operational Program Knowledge Education Development. MG and EBA thank Professor Artur Stefankiewicz for support. The computations were performed at the Poznań Supercomputing and Networking Center and supported in part by PL-Grid Infrastructure. AL acknowledges support from the Ministry of Science and Higher Education.

Funding information

Funding for this research was provided by: European Social Fund (grant No. POWR.03.02.00-00-I026/16).

References

Austin, A., Petersson, G. A., Frisch, M. J., Dobek, F. J., Scalmani, G. & Throssell, K. (2012). *J. Chem. Theory Comput.* **8**, 4989–5007.
Bader, R. F. W. (1994). In *Atoms in Molecules: A Quantum Theory*. Oxford, New York: Oxford University Press.
Banerjee, M. & Brettmann, B. (2020). *Pharmaceutics*, **12**, 995.
Bruno, I. J., Cole, J. C., Edgington, P. R., Kessler, M., Macrae, C. F., McCabe, P., Pearson, J. & Taylor, R. (2002). *Acta Cryst.* B**58**, 389–397.
Byrn, S. R., Zografi, G. & Chen, X. S. (2017). *Solid State Properties of Pharmaceutical Materials*, pp. 60–68. Hoboken: John Wiley & Sons.
Carstens, T., Haynes, D. A. & Smith, V. J. (2020). *Cryst. Growth Des.* **20**, 1139–1149.
Chumakov, Y., Simonov, Y., Grozav, M., Crisan, M., Bocelli, G., Yakovenko, A. & Lyubetsky, D. (2006). *Open Chem.* **4**, 458–475.
Clarke, H. D., Arora, K. K., Bass, H., Kavuru, P., Ong, T. T., Pujari, T., Wojtas, L. & Zaworotko, M. J. (2010). *Cryst. Growth Des.* **10**, 2152–2167.
Cruz-Cabeza, A. J. (2012). *CrystEngComm*, **14**, 6362–6365.
Dai, X.-L., Chen, J.-M. & Lu, T.-B. (2018). *CrystEngComm*, **20**, 5292–5316.
D'Ascenzo, L. & Auffinger, P. (2015). *Acta Cryst.* B**71**, 164–175.
Dolomanov, O. V., Bourhis, L. J., Gildea, R. J., Howard, J. A. K. & Puschmann, H. (2009). *J. Appl. Cryst.* **42**, 339–341.
Etter, M. C. (1990). *Acc. Chem. Res.* **23**, 120–126.
Fang, C.-H., Chen, P.-H., Chen, Y.-P. & Tang, M. (2020). *Chem. Eng. Technol.* **43**, 1186–1193.
Foresman, J. B. & Frisch, A. (2015). *Exploring Chemistry with Electronic Structure Methods*, 3rd ed. Wallingford, CT, USA: Gaussian Inc.
Frisch, M. J., *et al.* (2016). *GAUSSIAN16*. Gaussian Inc., Wallingford, CT, USA. https://gaussian.com/.
Gdaniec, M., Gilski, M. & Denisov, G. S. (1994). *Acta Cryst.* C**50**, 1622–1626.
Ghadi, R., Ghuge, A., Ghumre, S., Waghmare, N. & Kadam, D. V. J. (2014). *Indo Am. J. Pharm. Res.* **4**, 3881–3893.
Gołdyn, M., Larowska, D., Nowak, W. & Bartoszak-Adamska, E. (2019). *CrystEngComm*, **21**, 7373–7388.
Gołdyn, M. R., Larowska, D. & Bartoszak-Adamska, E. (2021). *Cryst. Growth Des.* **21**, 396–413.
Groom, C. R., Bruno, I. J., Lightfoot, M. P. & Ward, S. C. (2016). *Acta Cryst.* B**72**, 171–179.
Gunasekaran, S., Sankari, G. & Ponnusamy, S. (2005). *Spectrochim. Acta A*, **61**, 117–127.
Hancock, B. C. & Parks, M. (2000). *Pharm. Res.* **17**, 397–404.
Jacobs, A. & Amombo Noa, F. M. (2015). *CrystEngComm*, **17**, 98–106.
Jamróz, M. H. (2004). Vibrational Energy Distribution Analysis (*VEDA 4*) Program. Institute of Nuclear Chemistry and Technology, Warsaw, Poland.
Jamróz, M. H. (2013). *Spectrochim. Acta A*, **114**, 220–230.
Karki, S., Fábián, L., Friščić, T. & Jones, W. (2007). *Org. Lett.* **9**, 3133–3136.
Klímová, K. & Leitner, J. (2012). *Thermochim. Acta*, **550**, 59–64.
Kumar, R., Dalvi, S. V. & Siril, P. F. (2020). *ACS Appl. Nano Mater.* **3**, 4944–4961.
Kumar, S. & Nanda, A. (2018). *Indian J. Pharm. Sci.* **79**, 858–871.
Li, W., Shi, P., Jia, L., Zhao, Y., Sun, B., Zhang, M., Gong, J. & Tang, W. (2020). *J. Pharm. Sci.* **109**, 2224–2236.
Liao, X., Gautam, M., Grill, A. & Zhu, H. J. (2010). *J. Pharm. Sci.* **99**, 246–254.
Lilley, T. H., Linsdell, H. & Maestre, A. (1992). *J. Chem. Soc. Faraday Trans.* **88**, 2865–2870.
Lopez-Toledano, M. A., Saxena, V., Legassie, J. D., Liu, H., Ghanta, A., Riseman, S., Cocilova, C., Daak, A., Thorsteinsson, T., Rabinowicz, A. L. & Sancilio, F. D. (2019). *J. Drug. Deliv.* **2019**, 1–10.
Lu, T. & Chen, F. (2012). *J. Comput. Chem.* **33**, 580–592.
MacGillivray, L. R. & Zaworotko, M. J. (1994). *J. Chem. Crystallogr.* **24**, 703–705.
Macrae, C. F., Sovago, I., Cottrell, S. J., Galek, P. T. A., McCabe, P., Pidcock, E., Platings, M., Shields, G. P., Stevens, J. S., Towler, M. & Wood, P. A. (2020). *J. Appl. Cryst.* **53**, 226–235.
Martin, A., Paruta, A. N. & Adjei, A. (1981). *J. Pharm. Sci.* **70**, 1115–1120.
Nair, A. R., Lakshman, Y. D., Anand, V. S. K., Sree, K. S. N., Bhat, K. & Dengale, S. J. (2020). *AAPS PharmSciTech*, **21**, 309.
Papadopoulos, N. & Avranas, A. (1991). *J. Solution Chem.* **20**, 293–300.
Pehlivanov, I. (2020). *JofIMAB*, **26**, 3226–3233.
Pereira, J. F. B., Magri, A., Quental, M. V., Gonzalez-Miquel, M., Freire, M. G. & Coutinho, J. A. P. (2016). *ACS Sustainable Chem. Eng.* **4**, 1512–1520.
Rigaku OD (2019). *CrysAlis PRO*. Rigaku Oxford Diffraction Ltd, Yarnton, Oxfordshire, England.
Roy, P. & Ghosh, A. (2020). *CrystEngComm*, **22**, 6958–6974.
Sanphui, P. & Nangia, A. (2014). *J. Chem. Sci.* **126**, 1249–1264.
Sareen, S., Mathew, G. & Joseph, L. (2012). *Int. J. Pharm. Investig.* **2**, 12–17.
Sarma, B. & Saikia, B. (2014). *CrystEngComm*, **16**, 4753–4765.

Schultheiss, N. & Newman, A. (2009). *Cryst. Growth Des.* **9**, 2950–2967.
Shefter, E., Brennan, T. F. & Sackman, P. (1971). *Chem. Pharm. Bull.* **19**, 746–752.
Sheldrick, G. M. (2015*a*). *Acta Cryst.* A**71**, 3–8.
Sheldrick, G. M. (2015*b*). *Acta Cryst.* C**71**, 3–8.
Solomon, K. A., Blacque, O. & Venkatnarayan, R. (2017). *J. Mol. Struct.* **1134**, 190–198.
Srivastava, S. K. & Singh, V. B. (2013). *Spectrochim. Acta A*, **115**, 45–50.
Stefan, C., Martin, W., Finke, J. H., Kwade, A., van Eerdenbrugh, B., Juhnke, M. & Bunjes, H. (2020). *Eur. J. Pharm. Biopharm.* **152**, 63–71.
Wiberg, K. B. (1986). *J. Comput. Chem.* **7**, 379.
Yadav, A. V., Shete, A. S., Dabke, A. P., Kulkarni, P. V. & Sakhare, S. S. (2009). *Indian J. Pharm. Sci.* **71**, 359.
Yu, L. (2001). *Adv. Drug Deliv. Rev.* **48**, 27–42.

supporting information

Acta Cryst. (2021). C**77**, 713-724 [https://doi.org/10.1107/S2053229621010883]

Salts of purine alkaloids caffeine and theobromine with 2,6-dihydroxybenzoic acid as coformer: structural, theoretical, thermal and spectroscopic studies

Mateusz Gołdyn, Anna Komasa, Mateusz Pawlaczyk, Aneta Lewandowska and Elżbieta Bartoszak-Adamska

Computing details

For both structures, data collection: *CrysAlis PRO* (Rigaku OD, 2019); cell refinement: *CrysAlis PRO* (Rigaku OD, 2019); data reduction: *CrysAlis PRO* (Rigaku OD, 2019); program(s) used to solve structure: SHELXT2018 (Sheldrick, 2015a); program(s) used to refine structure: *SHELXL2018* (Sheldrick, 2015b); molecular graphics: OLEX2 (Dolomanov *et al.*, 2009); software used to prepare material for publication: OLEX2 (Dolomanov *et al.*, 2009).

1,3,7-Trimethyl-2,6-dioxo-2,3,6,9-tetrahydro-1*H*-purin-7-ium 2,6-dihydroxybenzoate (caf-26dhba-1-1b)

Crystal data

$C_8H_{11}N_4O_2^+ \cdot C_7H_5O_4^-$
M_r = 348.32
Monoclinic, $P2_1/n$
a = 14.8560 (3) Å
b = 6.95591 (11) Å
c = 15.8927 (3) Å
β = 115.413 (3)°
V = 1483.39 (6) Å^3
Z = 4
$F(000)$ = 728
D_x = 1.560 Mg m^{-3}
Melting point: 183 K
Cu $K\alpha$ radiation, λ = 1.54184 Å
Cell parameters from 6420 reflections
θ = 3.1–75.9°
μ = 1.05 mm^{-1}
T = 131 K
Block, clear light colourless
0.3 × 0.17 × 0.12 mm

Data collection

Rigaku OD SuperNova Single source diffractometer with an Atlas detector
Radiation source: micro-focus sealed X-ray tube, SuperNova (Cu) X-ray Source
Mirror monochromator
Detector resolution: 10.5357 pixels mm^{-1}
ω scans
Absorption correction: multi-scan (CrysAlis PRO; Rigaku OD, 2019)
T_{min} = 0.773, T_{max} = 1.000
11899 measured reflections
3076 independent reflections
2815 reflections with $I > 2\sigma(I)$
R_{int} = 0.025
θ_{max} = 76.4°, θ_{min} = 3.4°
h = −18→18
k = −8→8
l = −19→19

Refinement

Refinement on F^2
Least-squares matrix: full
$R[F^2 > 2\sigma(F^2)]$ = 0.034
$wR(F^2)$ = 0.096
S = 1.05
3076 reflections
290 parameters
1 restraint
Primary atom site location: dual
Hydrogen site location: difference Fourier map
All H-atom parameters refined

$w = 1/[\sigma^2(F_o^2) + (0.0539P)^2 + 0.4452P]$
where $P = (F_o^2 + 2F_c^2)/3$
$(\Delta/\sigma)_{max} < 0.001$

$\Delta\rho_{max} = 0.28$ e Å^{-3}
$\Delta\rho_{min} = -0.18$ e Å^{-3}

Special details

Geometry. All esds (except the esd in the dihedral angle between two l.s. planes) are estimated using the full covariance matrix. The cell esds are taken into account individually in the estimation of esds in distances, angles and torsion angles; correlations between esds in cell parameters are only used when they are defined by crystal symmetry. An approximate (isotropic) treatment of cell esds is used for estimating esds involving l.s. planes.

Fractional atomic coordinates and isotropic or equivalent isotropic displacement parameters (Å²)

	x	*y*	*z*	U_{iso}*/U_{eq}
O6	0.87775 (7)	0.94531 (14)	0.71150 (6)	0.0295 (2)
O5	0.80375 (7)	1.01841 (13)	0.40182 (6)	0.0266 (2)
N2	0.72024 (8)	0.86953 (15)	0.60787 (7)	0.0224 (2)
N4	0.55934 (7)	0.79191 (15)	0.48111 (7)	0.0232 (2)
H4	0.5168 (15)	0.752 (3)	0.5118 (15)	0.064 (6)*
N1	0.83843 (7)	0.98771 (15)	0.55706 (7)	0.0228 (2)
N3	0.59383 (8)	0.86753 (15)	0.36370 (7)	0.0228 (2)
C9	0.81589 (9)	0.93483 (17)	0.63069 (8)	0.0231 (3)
C11	0.67820 (9)	0.90751 (17)	0.44496 (8)	0.0216 (2)
C12	0.52493 (9)	0.79891 (18)	0.38801 (9)	0.0247 (3)
H12	0.4601 (12)	0.758 (2)	0.3432 (11)	0.027 (4)*
C10	0.65472 (9)	0.85802 (17)	0.51619 (8)	0.0214 (2)
C8	0.77546 (9)	0.97551 (17)	0.46063 (8)	0.0217 (2)
C15	0.94090 (9)	1.0539 (2)	0.58291 (9)	0.0281 (3)
H15A	0.9644 (16)	1.126 (3)	0.6409 (16)	0.056 (6)*
H15B	0.9400 (16)	1.136 (3)	0.5311 (15)	0.052 (6)*
H15C	0.9864 (18)	0.947 (3)	0.5919 (16)	0.064 (7)*
C13	0.69146 (10)	0.8075 (2)	0.68087 (9)	0.0281 (3)
H13A	0.7503 (14)	0.808 (3)	0.7393 (13)	0.037 (5)*
H13B	0.6421 (16)	0.902 (3)	0.6872 (15)	0.054 (6)*
H13C	0.6599 (16)	0.680 (3)	0.6668 (14)	0.050 (5)*
C14	0.58116 (10)	0.8956 (2)	0.26772 (9)	0.0282 (3)
H14A	0.6294 (14)	0.818 (3)	0.2556 (13)	0.044 (5)*
H14B	0.5940 (16)	1.030 (3)	0.2598 (14)	0.049 (5)*
H14C	0.5130 (16)	0.864 (3)	0.2249 (15)	0.050 (5)*
O4	0.16405 (7)	0.53913 (15)	0.37731 (6)	0.0297 (2)
H4A	0.2180 (16)	0.593 (3)	0.3738 (14)	0.047 (5)*
O2	0.45129 (6)	0.69157 (14)	0.56176 (6)	0.0275 (2)
O1	0.33645 (7)	0.67306 (15)	0.41487 (6)	0.0298 (2)
O3	0.40547 (7)	0.61533 (16)	0.69704 (6)	0.0311 (2)
H3	0.4443 (17)	0.645 (3)	0.6650 (16)	0.061 (6)*
C1	0.28984 (9)	0.58156 (17)	0.53489 (8)	0.0221 (2)
C6	0.19273 (9)	0.52601 (18)	0.47030 (9)	0.0237 (3)
C2	0.31443 (9)	0.56542 (18)	0.63089 (9)	0.0236 (3)
C5	0.12501 (9)	0.45492 (19)	0.50127 (9)	0.0268 (3)
H5	0.0609 (13)	0.417 (2)	0.4566 (12)	0.029 (4)*

C3	0.24597 (10)	0.49508 (19)	0.66139 (9)	0.0271 (3)
H3A	0.2650 (14)	0.486 (3)	0.7277 (13)	0.036 (5)*
C7	0.36193 (9)	0.65282 (18)	0.50043 (9)	0.0233 (3)
C4	0.15242 (10)	0.43917 (19)	0.59610 (10)	0.0281 (3)
H4B	0.1039 (13)	0.389 (2)	0.6177 (12)	0.033 (4)*

Atomic displacement parameters (Å²)

	U^{11}	U^{22}	U^{33}	U^{12}	U^{13}	U^{23}
O6	0.0235 (4)	0.0408 (5)	0.0193 (4)	−0.0023 (4)	0.0045 (4)	0.0005 (4)
O5	0.0259 (4)	0.0328 (5)	0.0220 (4)	−0.0026 (4)	0.0112 (4)	0.0004 (3)
N2	0.0208 (5)	0.0277 (5)	0.0169 (5)	−0.0002 (4)	0.0065 (4)	0.0007 (4)
N4	0.0194 (5)	0.0273 (5)	0.0212 (5)	−0.0009 (4)	0.0072 (4)	0.0003 (4)
N1	0.0191 (5)	0.0276 (5)	0.0198 (5)	−0.0008 (4)	0.0065 (4)	−0.0002 (4)
N3	0.0202 (5)	0.0278 (5)	0.0178 (5)	−0.0002 (4)	0.0058 (4)	−0.0003 (4)
C9	0.0217 (6)	0.0245 (6)	0.0211 (6)	0.0018 (4)	0.0073 (5)	−0.0001 (4)
C11	0.0204 (6)	0.0240 (6)	0.0179 (5)	0.0009 (4)	0.0058 (4)	0.0002 (4)
C12	0.0202 (6)	0.0288 (6)	0.0225 (6)	−0.0006 (5)	0.0066 (5)	−0.0006 (5)
C10	0.0193 (5)	0.0232 (5)	0.0196 (6)	0.0011 (4)	0.0065 (4)	0.0000 (4)
C8	0.0212 (6)	0.0225 (5)	0.0198 (6)	0.0009 (4)	0.0073 (5)	0.0000 (4)
C15	0.0191 (6)	0.0375 (7)	0.0260 (6)	−0.0036 (5)	0.0081 (5)	−0.0008 (5)
C13	0.0253 (6)	0.0385 (7)	0.0203 (6)	−0.0020 (5)	0.0096 (5)	0.0017 (5)
C14	0.0266 (6)	0.0381 (7)	0.0177 (6)	−0.0017 (5)	0.0074 (5)	0.0012 (5)
O4	0.0249 (5)	0.0404 (5)	0.0206 (4)	−0.0012 (4)	0.0066 (4)	−0.0021 (4)
O2	0.0209 (4)	0.0368 (5)	0.0238 (4)	−0.0024 (4)	0.0088 (3)	0.0004 (4)
O1	0.0284 (5)	0.0407 (5)	0.0208 (4)	−0.0019 (4)	0.0109 (4)	0.0012 (4)
O3	0.0223 (4)	0.0476 (6)	0.0204 (4)	−0.0025 (4)	0.0064 (4)	−0.0009 (4)
C1	0.0204 (6)	0.0239 (6)	0.0215 (6)	0.0017 (4)	0.0084 (5)	0.0003 (4)
C6	0.0218 (6)	0.0247 (6)	0.0227 (6)	0.0029 (5)	0.0078 (5)	−0.0016 (5)
C2	0.0207 (6)	0.0267 (6)	0.0218 (6)	0.0031 (4)	0.0076 (5)	0.0002 (4)
C5	0.0205 (6)	0.0298 (6)	0.0286 (6)	−0.0002 (5)	0.0091 (5)	−0.0032 (5)
C3	0.0274 (6)	0.0320 (6)	0.0241 (6)	0.0033 (5)	0.0131 (5)	0.0020 (5)
C7	0.0230 (6)	0.0243 (6)	0.0226 (6)	0.0016 (4)	0.0097 (5)	−0.0004 (4)
C4	0.0256 (6)	0.0303 (6)	0.0321 (7)	0.0013 (5)	0.0160 (5)	0.0009 (5)

Geometric parameters (Å, º)

O6—C9	1.2191 (16)	C13—H13B	1.02 (2)
O5—C8	1.2151 (16)	C13—H13C	0.98 (2)
N2—C9	1.3838 (16)	C14—H14A	0.98 (2)
N2—C10	1.3636 (16)	C14—H14B	0.97 (2)
N2—C13	1.4631 (16)	C14—H14C	0.97 (2)
N4—H4	0.989 (15)	O4—H4A	0.91 (2)
N4—C12	1.3431 (16)	O4—C6	1.3541 (16)
N4—C10	1.3608 (16)	O2—C7	1.2940 (15)
N1—C9	1.3976 (16)	O1—C7	1.2530 (16)
N1—C8	1.4144 (15)	O3—H3	0.94 (2)
N1—C15	1.4700 (16)	O3—C2	1.3545 (15)

N3—C11	1.3882 (15)	C1—C6	1.4189 (17)
N3—C12	1.3282 (16)	C1—C2	1.4125 (17)
N3—C14	1.4677 (15)	C1—C7	1.4821 (17)
C11—C10	1.3641 (17)	C6—C5	1.3870 (18)
C11—C8	1.4369 (17)	C2—C3	1.3900 (18)
C12—H12	0.963 (16)	C5—H5	0.949 (18)
C15—H15A	0.97 (2)	C5—C4	1.3865 (19)
C15—H15B	1.00 (2)	C3—H3A	0.970 (19)
C15—H15C	0.97 (2)	C3—C4	1.3862 (19)
C13—H13A	0.964 (19)	C4—H4B	0.985 (18)

C9—N2—C13	120.37 (10)	N2—C13—H13B	110.8 (12)
C10—N2—C9	118.77 (10)	N2—C13—H13C	111.1 (12)
C10—N2—C13	120.82 (10)	H13A—C13—H13B	107.1 (16)
C12—N4—H4	122.1 (13)	H13A—C13—H13C	111.6 (16)
C12—N4—C10	106.04 (10)	H13B—C13—H13C	108.1 (17)
C10—N4—H4	131.8 (13)	N3—C14—H14A	110.6 (11)
C9—N1—C8	127.35 (10)	N3—C14—H14B	108.5 (12)
C9—N1—C15	116.09 (10)	N3—C14—H14C	109.2 (12)
C8—N1—C15	116.47 (10)	H14A—C14—H14B	107.8 (17)
C11—N3—C14	127.02 (10)	H14A—C14—H14C	111.6 (16)
C12—N3—C11	107.59 (10)	H14B—C14—H14C	109.1 (17)
C12—N3—C14	125.38 (11)	C6—O4—H4A	102.8 (13)
O6—C9—N2	121.39 (12)	C2—O3—H3	106.0 (14)
O6—C9—N1	121.55 (11)	C6—C1—C7	119.69 (11)
N2—C9—N1	117.06 (10)	C2—C1—C6	118.11 (11)
N3—C11—C8	131.80 (11)	C2—C1—C7	122.19 (11)
C10—C11—N3	105.73 (10)	O4—C6—C1	121.15 (11)
C10—C11—C8	122.38 (11)	O4—C6—C5	118.35 (11)
N4—C12—H12	126.2 (9)	C5—C6—C1	120.49 (12)
N3—C12—N4	110.91 (11)	O3—C2—C1	121.83 (11)
N3—C12—H12	122.8 (9)	O3—C2—C3	117.11 (11)
N2—C10—C11	123.53 (11)	C3—C2—C1	121.05 (12)
N4—C10—N2	126.72 (11)	C6—C5—H5	118.8 (10)
N4—C10—C11	109.72 (11)	C4—C5—C6	119.64 (12)
O5—C8—N1	122.17 (11)	C4—C5—H5	121.6 (10)
O5—C8—C11	126.98 (11)	C2—C3—H3A	119.1 (11)
N1—C8—C11	110.85 (10)	C4—C3—C2	119.10 (12)
N1—C15—H15A	109.6 (13)	C4—C3—H3A	121.8 (11)
N1—C15—H15B	107.6 (12)	O2—C7—C1	117.50 (11)
N1—C15—H15C	111.9 (14)	O1—C7—O2	121.91 (11)
H15A—C15—H15B	111.0 (17)	O1—C7—C1	120.59 (11)
H15A—C15—H15C	108.1 (19)	C5—C4—H4B	119.3 (10)
H15B—C15—H15C	108.7 (18)	C3—C4—C5	121.59 (12)
N2—C13—H13A	108.1 (11)	C3—C4—H4B	119.1 (10)

N3—C11—C10—N2	177.45 (11)	C13—N2—C9—O6	−1.19 (19)
N3—C11—C10—N4	−0.66 (14)	C13—N2—C9—N1	178.67 (11)

N3—C11—C8—O5	2.1 (2)	C13—N2—C10—N4	0.05 (19)
N3—C11—C8—N1	−177.84 (12)	C13—N2—C10—C11	−177.73 (12)
C9—N2—C10—N4	177.81 (11)	C14—N3—C11—C10	−179.96 (12)
C9—N2—C10—C11	0.03 (18)	C14—N3—C11—C8	−3.4 (2)
C9—N1—C8—O5	−176.99 (12)	C14—N3—C12—N4	−179.58 (11)
C9—N1—C8—C11	2.91 (17)	O4—C6—C5—C4	179.76 (12)
C11—N3—C12—N4	0.14 (14)	O3—C2—C3—C4	−178.92 (12)
C12—N4—C10—N2	−177.29 (12)	C1—C6—C5—C4	0.36 (19)
C12—N4—C10—C11	0.75 (14)	C1—C2—C3—C4	0.36 (19)
C12—N3—C11—C10	0.32 (14)	C6—C1—C2—O3	179.98 (11)
C12—N3—C11—C8	176.88 (13)	C6—C1—C2—C3	0.73 (18)
C10—N2—C9—O6	−178.96 (12)	C6—C1—C7—O2	−176.21 (11)
C10—N2—C9—N1	0.89 (17)	C6—C1—C7—O1	3.39 (18)
C10—N4—C12—N3	−0.55 (14)	C6—C5—C4—C3	0.8 (2)
C10—C11—C8—O5	178.14 (12)	C2—C1—C6—O4	179.52 (11)
C10—C11—C8—N1	−1.76 (17)	C2—C1—C6—C5	−1.10 (18)
C8—N1—C9—O6	177.25 (12)	C2—C1—C7—O2	3.42 (18)
C8—N1—C9—N2	−2.60 (18)	C2—C1—C7—O1	−176.98 (12)
C8—C11—C10—N2	0.49 (19)	C2—C3—C4—C5	−1.1 (2)
C8—C11—C10—N4	−177.62 (11)	C7—C1—C6—O4	−0.84 (18)
C15—N1—C9—O6	0.73 (18)	C7—C1—C6—C5	178.55 (11)
C15—N1—C9—N2	−179.12 (11)	C7—C1—C2—O3	0.35 (19)
C15—N1—C8—O5	−0.48 (18)	C7—C1—C2—C3	−178.90 (12)
C15—N1—C8—C11	179.42 (11)		

Hydrogen-bond geometry (Å, º)

D—H···*A*	*D*—H	H···*A*	*D*···*A*	*D*—H···*A*
N4—H4···O2	0.99 (2)	1.56 (2)	2.5441 (14)	179 (2)
O4—H4*A*···O1	0.91 (2)	1.69 (2)	2.5440 (13)	156.1 (19)
O3—H3···O2	0.94 (2)	1.72 (2)	2.5737 (13)	149 (2)

3,7-Dimethyl-2,6-dioxo-2,3,6,9-tetrahydro-1*H*-purin-7-ium 2,6-dihydroxybenzoate (tbr-26dhba-lag-cryst)

Crystal data

$C_7H_9N_4O_2^+·C_7H_5O_4^-$
M_r = 334.29
Monoclinic, $P2_1/c$
a = 6.9579 (3) Å
b = 16.5845 (6) Å
c = 12.4718 (5) Å
β = 95.691 (4)°
V = 1432.06 (10) Å^3
Z = 4
$F(000)$ = 696
D_x = 1.551 Mg m^{-3}
Melting point: 202 K
Cu $K\alpha$ radiation, λ = 1.54184 Å
Cell parameters from 5599 reflections
θ = 2.7–75.3°
μ = 1.06 mm^{-1}
T = 132 K
Plate, clear light colourless
0.34 × 0.24 × 0.08 mm

Data collection

Rigaku OD SuperNova Single source diffractometer with an Atlas detector
Radiation source: micro-focus sealed X-ray tube, SuperNova (Cu) X-ray Source
Mirror monochromator
Detector resolution: 10.5357 pixels mm^{-1}
ω scans
Absorption correction: multi-scan (CrysAlis PRO; Rigaku OD, 2019)
T_{min} = 0.649, T_{max} = 1.000
12055 measured reflections
2970 independent reflections
2782 reflections with $I > 2\sigma(I)$
R_{int} = 0.023
θ_{max} = 76.5°, θ_{min} = 4.5°
h = −8→8
k = −20→20
l = −15→15

Refinement

Refinement on F^2
Least-squares matrix: full
$R[F^2 > 2\sigma(F^2)]$ = 0.055
$wR(F^2)$ = 0.147
S = 1.11
2970 reflections
273 parameters
2 restraints
Primary atom site location: dual
Hydrogen site location: difference Fourier map
All H-atom parameters refined
$w = 1/[\sigma^2(F_o^2) + (0.0629P)^2 + 1.3861P]$ where $P = (F_o^2 + 2F_c^2)/3$
$(\Delta/\sigma)_{max} < 0.001$
$\Delta\rho_{max}$ = 0.51 e Å^{-3}
$\Delta\rho_{min}$ = −0.24 e Å^{-3}

Special details

Geometry. All esds (except the esd in the dihedral angle between two l.s. planes) are estimated using the full covariance matrix. The cell esds are taken into account individually in the estimation of esds in distances, angles and torsion angles; correlations between esds in cell parameters are only used when they are defined by crystal symmetry. An approximate (isotropic) treatment of cell esds is used for estimating esds involving l.s. planes.

Fractional atomic coordinates and isotropic or equivalent isotropic displacement parameters (Å^2)

	x	y	z	U_{iso}*/U_{eq}
O5	0.3845 (2)	0.28563 (9)	0.10648 (12)	0.0343 (4)
O6	0.4508 (2)	0.55891 (9)	0.10181 (12)	0.0315 (4)
O1	0.1578 (2)	0.43520 (9)	0.65282 (13)	0.0352 (4)
O2	0.2341 (2)	0.53812 (9)	0.55146 (12)	0.0327 (4)
O4	0.0791 (3)	0.45956 (11)	0.84553 (13)	0.0393 (4)
O3	0.2082 (3)	0.68358 (10)	0.61672 (14)	0.0394 (4)
N4	0.2886 (2)	0.42798 (11)	0.41420 (14)	0.0255 (4)
N1	0.4179 (3)	0.42264 (11)	0.10880 (14)	0.0265 (4)
N2	0.3665 (2)	0.50484 (10)	0.25777 (13)	0.0260 (4)
N3	0.3021 (3)	0.30658 (10)	0.34625 (14)	0.0289 (4)
C10	0.3345 (3)	0.43505 (12)	0.31106 (16)	0.0246 (4)
C11	0.3441 (3)	0.36048 (12)	0.26700 (16)	0.0260 (4)
C9	0.4144 (3)	0.49925 (13)	0.15252 (16)	0.0258 (4)
C8	0.3822 (3)	0.34889 (13)	0.15611 (16)	0.0261 (4)
C1	0.1489 (3)	0.56751 (13)	0.72638 (16)	0.0264 (4)
C7	0.1804 (3)	0.50870 (13)	0.64013 (16)	0.0267 (4)
C12	0.2705 (3)	0.34930 (13)	0.43346 (17)	0.0289 (4)
C2	0.1672 (3)	0.65122 (14)	0.71212 (18)	0.0310 (5)
C6	0.1026 (3)	0.53936 (14)	0.82804 (17)	0.0301 (5)
C13	0.3495 (4)	0.58438 (14)	0.30785 (19)	0.0336 (5)
C3	0.1432 (4)	0.70363 (15)	0.7959 (2)	0.0400 (6)

C5	0.0812 (3)	0.59200 (16)	0.91215 (19)	0.0368 (5)
C14	0.3021 (5)	0.21876 (14)	0.3388 (2)	0.0448 (6)
C4	0.1032 (4)	0.67333 (17)	0.8954 (2)	0.0425 (6)
H4B	0.077 (3)	0.7075 (14)	0.9512 (19)	0.022 (5)*
H1	0.454 (4)	0.4211 (16)	0.046 (2)	0.034 (7)*
H3	0.224 (5)	0.6347 (12)	0.575 (2)	0.057 (9)*
H3A	0.151 (4)	0.757 (2)	0.777 (2)	0.049 (8)*
H5	0.053 (4)	0.5737 (17)	0.980 (2)	0.040 (7)*
H14A	0.251 (5)	0.2049 (19)	0.262 (3)	0.056 (9)*
H13A	0.329 (4)	0.623 (2)	0.251 (3)	0.054 (9)*
H13B	0.232 (5)	0.5860 (19)	0.344 (3)	0.057 (9)*
H14B	0.225 (5)	0.198 (2)	0.398 (3)	0.064 (10)*
H4A	0.107 (5)	0.434 (2)	0.776 (3)	0.074 (11)*
H13C	0.457 (5)	0.595 (2)	0.356 (3)	0.061 (10)*
H4	0.273 (5)	0.473 (2)	0.459 (3)	0.081 (12)*
H14C	0.429 (6)	0.203 (2)	0.347 (3)	0.083 (13)*
H12	0.236 (4)	0.3280 (16)	0.5011 (13)	0.042 (7)*

Atomic displacement parameters (Å²)

	U^{11}	U^{22}	U^{33}	U^{12}	U^{13}	U^{23}
O5	0.0441 (9)	0.0314 (8)	0.0282 (8)	−0.0026 (7)	0.0069 (6)	−0.0048 (6)
O6	0.0389 (8)	0.0325 (8)	0.0241 (7)	−0.0070 (6)	0.0073 (6)	0.0025 (6)
O1	0.0443 (9)	0.0289 (8)	0.0333 (8)	0.0019 (6)	0.0087 (7)	−0.0001 (6)
O2	0.0429 (9)	0.0325 (8)	0.0238 (7)	−0.0004 (6)	0.0095 (6)	−0.0014 (6)
O4	0.0461 (9)	0.0401 (9)	0.0335 (9)	0.0068 (7)	0.0136 (7)	0.0100 (7)
O3	0.0526 (10)	0.0293 (8)	0.0379 (9)	−0.0032 (7)	0.0133 (7)	0.0044 (7)
N4	0.0262 (8)	0.0295 (9)	0.0213 (8)	0.0000 (7)	0.0043 (6)	0.0003 (7)
N1	0.0284 (8)	0.0324 (9)	0.0192 (8)	−0.0043 (7)	0.0053 (6)	−0.0010 (7)
N2	0.0295 (8)	0.0266 (9)	0.0225 (8)	−0.0026 (7)	0.0051 (6)	0.0007 (6)
N3	0.0384 (10)	0.0250 (9)	0.0234 (8)	0.0010 (7)	0.0034 (7)	0.0003 (7)
C10	0.0203 (9)	0.0307 (10)	0.0227 (9)	0.0005 (7)	0.0022 (7)	0.0007 (7)
C11	0.0259 (9)	0.0296 (10)	0.0225 (10)	−0.0007 (8)	0.0028 (7)	0.0050 (8)
C9	0.0229 (9)	0.0318 (10)	0.0226 (9)	−0.0033 (7)	0.0009 (7)	−0.0001 (8)
C8	0.0254 (9)	0.0298 (10)	0.0229 (9)	−0.0017 (8)	0.0018 (7)	−0.0020 (8)
C1	0.0208 (9)	0.0329 (11)	0.0253 (10)	0.0005 (7)	0.0009 (7)	−0.0005 (8)
C7	0.0228 (9)	0.0325 (10)	0.0249 (10)	0.0014 (8)	0.0026 (7)	−0.0037 (8)
C12	0.0334 (11)	0.0317 (10)	0.0219 (10)	0.0010 (8)	0.0044 (8)	0.0014 (8)
C2	0.0279 (10)	0.0338 (11)	0.0316 (11)	−0.0023 (8)	0.0037 (8)	−0.0011 (9)
C6	0.0226 (9)	0.0413 (12)	0.0264 (10)	0.0040 (8)	0.0031 (7)	0.0036 (9)
C13	0.0415 (13)	0.0282 (11)	0.0324 (11)	0.0005 (9)	0.0110 (10)	−0.0020 (9)
C3	0.0395 (13)	0.0297 (12)	0.0520 (15)	−0.0028 (9)	0.0094 (11)	−0.0071 (10)
C5	0.0283 (11)	0.0547 (15)	0.0274 (11)	0.0026 (10)	0.0030 (8)	0.0006 (10)
C14	0.077 (2)	0.0237 (11)	0.0345 (13)	0.0023 (12)	0.0092 (13)	−0.0007 (9)
C4	0.0363 (12)	0.0553 (15)	0.0363 (12)	−0.0009 (11)	0.0056 (10)	−0.0185 (12)

Geometric parameters (Å, º)

O5—C8	1.219 (3)	C10—C11	1.358 (3)
O6—C9	1.215 (3)	C11—C8	1.447 (3)
O1—C7	1.241 (3)	C1—C7	1.484 (3)
O2—C7	1.297 (3)	C1—C2	1.407 (3)
O4—C6	1.354 (3)	C1—C6	1.418 (3)
O4—H4A	1.00 (4)	C12—H12	0.966 (10)
O3—C2	1.361 (3)	C2—C3	1.382 (3)
O3—H3	0.975 (10)	C6—C5	1.384 (3)
N4—C10	1.361 (3)	C13—H13A	0.95 (3)
N4—C12	1.335 (3)	C13—H13B	0.97 (3)
N4—H4	0.94 (4)	C13—H13C	0.93 (4)
N1—C9	1.384 (3)	C3—C4	1.391 (4)
N1—C8	1.391 (3)	C3—H3A	0.92 (3)
N1—H1	0.85 (3)	C5—C4	1.376 (4)
N2—C10	1.364 (3)	C5—H5	0.94 (3)
N2—C9	1.389 (3)	C14—H14A	1.02 (3)
N2—C13	1.469 (3)	C14—H14B	1.01 (4)
N3—C11	1.385 (3)	C14—H14C	0.92 (4)
N3—C12	1.334 (3)	C4—H4B	0.93 (2)
N3—C14	1.460 (3)		

C6—O4—H4A	104 (2)	O2—C7—C1	116.52 (18)
C2—O3—H3	101 (2)	N4—C12—H12	123.4 (17)
C10—N4—H4	123 (2)	N3—C12—N4	110.26 (18)
C12—N4—C10	106.82 (17)	N3—C12—H12	126.3 (17)
C12—N4—H4	131 (2)	O3—C2—C1	121.9 (2)
C9—N1—C8	128.99 (17)	O3—C2—C3	117.7 (2)
C9—N1—H1	114.3 (18)	C3—C2—C1	120.4 (2)
C8—N1—H1	116.6 (18)	O4—C6—C1	120.51 (19)
C10—N2—C9	118.03 (17)	O4—C6—C5	118.1 (2)
C10—N2—C13	122.05 (17)	C5—C6—C1	121.4 (2)
C9—N2—C13	119.91 (17)	N2—C13—H13A	106.9 (19)
C11—N3—C14	126.65 (19)	N2—C13—H13B	109.3 (19)
C12—N3—C11	107.60 (17)	N2—C13—H13C	111 (2)
C12—N3—C14	125.67 (19)	H13A—C13—H13B	105 (3)
N4—C10—N2	126.78 (19)	H13A—C13—H13C	114 (3)
C11—C10—N4	109.25 (18)	H13B—C13—H13C	111 (3)
C11—C10—N2	123.97 (18)	C2—C3—C4	119.8 (2)
N3—C11—C8	131.92 (19)	C2—C3—H3A	113 (2)
C10—C11—N3	106.06 (17)	C4—C3—H3A	127 (2)
C10—C11—C8	121.94 (18)	C6—C5—H5	121.8 (17)
O6—C9—N1	122.00 (18)	C4—C5—C6	118.8 (2)
O6—C9—N2	121.32 (19)	C4—C5—H5	119.4 (17)
N1—C9—N2	116.69 (17)	N3—C14—H14A	106.5 (18)
O5—C8—N1	121.97 (19)	N3—C14—H14B	107 (2)
O5—C8—C11	127.8 (2)	N3—C14—H14C	106 (3)

N1—C8—C11	110.24 (17)	H14A—C14—H14B	116 (3)
C2—C1—C7	122.34 (19)	H14A—C14—H14C	106 (3)
C2—C1—C6	117.99 (19)	H14B—C14—H14C	114 (3)
C6—C1—C7	119.65 (19)	C3—C4—H4B	121.2 (15)
O1—C7—O2	121.94 (19)	C5—C4—C3	121.6 (2)
O1—C7—C1	121.54 (19)	C5—C4—H4B	116.9 (14)
O4—C6—C5—C4	−179.5 (2)	C7—C1—C6—O4	−2.7 (3)
O3—C2—C3—C4	−179.3 (2)	C7—C1—C6—C5	176.86 (19)
N4—C10—C11—N3	0.2 (2)	C12—N4—C10—N2	−179.93 (19)
N4—C10—C11—C8	177.29 (18)	C12—N4—C10—C11	0.1 (2)
N2—C10—C11—N3	−179.78 (18)	C12—N3—C11—C10	−0.4 (2)
N2—C10—C11—C8	−2.6 (3)	C12—N3—C11—C8	−177.1 (2)
N3—C11—C8—O5	0.3 (4)	C2—C1—C7—O1	−177.7 (2)
N3—C11—C8—N1	−179.8 (2)	C2—C1—C7—O2	2.8 (3)
C10—N4—C12—N3	−0.4 (2)	C2—C1—C6—O4	178.56 (19)
C10—N2—C9—O6	−177.57 (18)	C2—C1—C6—C5	−1.9 (3)
C10—N2—C9—N1	2.5 (3)	C2—C3—C4—C5	−1.9 (4)
C10—C11—C8—O5	−176.0 (2)	C6—C1—C7—O1	3.6 (3)
C10—C11—C8—N1	3.9 (3)	C6—C1—C7—O2	−175.85 (18)
C11—N3—C12—N4	0.5 (2)	C6—C1—C2—O3	−178.87 (19)
C9—N1—C8—O5	177.6 (2)	C6—C1—C2—C3	1.0 (3)
C9—N1—C8—C11	−2.2 (3)	C6—C5—C4—C3	1.0 (4)
C9—N2—C10—N4	179.22 (18)	C13—N2—C10—N4	−1.6 (3)
C9—N2—C10—C11	−0.9 (3)	C13—N2—C10—C11	178.3 (2)
C8—N1—C9—O6	179.2 (2)	C13—N2—C9—O6	3.2 (3)
C8—N1—C9—N2	−0.9 (3)	C13—N2—C9—N1	−176.72 (18)
C1—C2—C3—C4	0.9 (4)	C14—N3—C11—C10	−177.3 (2)
C1—C6—C5—C4	0.9 (3)	C14—N3—C11—C8	5.9 (4)
C7—C1—C2—O3	2.4 (3)	C14—N3—C12—N4	177.5 (2)
C7—C1—C2—C3	−177.7 (2)		

Hydrogen-bond geometry (Å, º)

D—H···*A*	*D*—H	H···*A*	*D*···*A*	*D*—H···*A*
N1—H1···O6^{i}	0.85 (3)	2.04 (3)	2.881 (2)	169 (3)
O3—H3···O2	0.98 (1)	1.63 (2)	2.558 (2)	157 (3)
O4—H4*A*···O1	1.00 (4)	1.62 (4)	2.550 (2)	153 (3)
N4—H4···O2	0.94 (4)	1.62 (4)	2.557 (2)	169 (4)

Symmetry code: (i) −*x*+1, −*y*+1, −*z*.